Journal of Inorganic Biochemistry 260 (2024) 112697

Contents lists available at ScienceDirect

Journal of Inorganic Biochemistry

journal homepage: www.elsevier.com/locate/jinorgbio

Dimolybdenum (II,II) paddlewheel complexes bearing non-steroidal anti-inflammatory drug ligands: Insights into the chemico-physical profile and first biological assessment

Lorenzo Chiaverini [a], Valentina Notarstefano [b,*], Iogann Tolbatov [c,d,*], Paolo Umari [c], Elisabetta Giorgini [b], Lidia Ciccone [a], Riccardo Di Leo [a], Letizia Trincavelli [a], Chiara Giacomelli [a], Laura Marchetti [a], Tiziano Marzo [a,*], Diego La Mendola [a], Alessandro Marrone [e]

[a] Department of Pharmacy, University of Pisa, Via Bonanno Pisano 6, 56126 Pisa, Italy
[b] Department of Life and Environmental Sciences, DiSVA, Università Politecnica delle Marche, Via Brecce Bianche, 60131 Ancona, Italy
[c] Department of Physics and Astronomy, University of Padova, via F. Marzolo 8, 35131 Padova, Italy
[d] Institute of Chemical Research of Catalonia (ICIQ), The Barcelona Institute of Science and Technology, av. Paisos Catalans 16, 43007 Tarragona, Spain
[e] Dipartimento di Farmacia, Università degli Studi "G. D'Annunzio" Chieti-Pescara, Via dei Vestini, 66100 Chieti, Italy

ARTICLE INFO

Keywords:
Paddlewheel dinuclear complexes
NSAIDs
Dimolybdenum
Metal-based complexes
Cancer

ABSTRACT

Multinuclear complexes are metal compounds featured by adjacent bound metal centers that can lead to unconventional reactivity. Some M_2L_4-type paddlewheel dinuclear complexes with monoanionic bridging ligands feature promising properties, including therapeutic ones. Molybdenum has been studied for the formation of multiple-bonded M^{2+} compounds due to their unique scaffold, redox, and spectroscopic properties as well as for applications in several fields including catalysis and biology. These latter are much less explored and only sporadic studies have been carried out. Here, a series of four dimolybdenum (II,II) carboxylate paddlewheel complexes were synthesized using different Non-Steroidal Anti-Inflammatory Drugs (NSAIDs) as ligands. The reaction of $(NH_4)_5[Mo_2Cl_9]\cdot H_2O$ with the selected NSAIDs in methanol produced the complexes $Mo_2(\mu\text{-}O_2CR)_4$ where RCO_2 is ibuprofen (**1**), naproxen (**2**), aspirin (**3**) and indomethacin (**4**). The products were obtained in good yields and extensively characterized with integrated techniques. Stability and solution behaviour were studied using a mixed experimental and computational approach. Finally, the biological activity of **1** and **3** (i.e. the most reactive and the most stable compounds of the series, respectively) was preliminarily assessed confirming the disassembling of the molecules in the biological milieu. Overall, some very interesting results emerged for these unconventional compounds from a mechanistic point of view.

1. Introduction

Metal-based complexes, bearing a dimetallic center in which two metal ions are directly connected, represent a family of inorganic molecules employed in various chemistry domains, including catalysis [1], 3D network structured molecular magnets preparation [2], and medicinal applications [3]. Specifically, paddlewheel complexes have attracted attention in the last decades [4–6] due to their unique chemical features and peculiar geometry. Indeed, some of these compounds are extensively used as industrial catalysts. This is the case, for instance, of some dirhodium (II,II) compounds, which are also exploited as building blocks for molecular scaffolds [7]. Furthermore, these complexes find application in organic synthesis where they are commonly used to transfer electron-deficient species, act as Lewis acids for the activation of unsaturated bonds, serve as hydrogenation catalysts, and participate in redox processes [7]. Similarly, mixed-valence ruthenium (II,III) compounds find application in various research and industrial fields [8]. Paddlewheel compounds featured by the presence of essential metals were also reported. Among them various copper(II) carboxylates, some of which bearing Non-Steroidal Anti-Inflammatory Drugs (NSAID)

* Corresponding authors at: Department of Pharmacy, University of Pisa, Via Bonanno Pisano 6, 56126 Pisa, Italy (T. Marzo); Department of Physics and Astronomy, University of Padova, via F. Marzolo 8, 35131 Padova, Italy (I. Tolbatov).
E-mail addresses: v.notarstefano@staff.univpm.it (V. Notarstefano), tolbatov.i@gmail.com (I. Tolbatov), tiziano.marzo@unipi.it (T. Marzo).

https://doi.org/10.1016/j.jinorgbio.2024.112697
Received 24 June 2024; Received in revised form 25 July 2024; Accepted 11 August 2024
Available online 12 August 2024

ligands showed interesting features suitable for potential medicinal application [9–19]. For instance, the ability to interact and coordinate biological substrates such as proteins or DNA was previously reported [10]. Interestingly, the paddlewheel geometry, combined with the presence of a dimetallic core, makes these systems of potential interest for medicinal application. Hence, through the accurate choice of the dimetallic core and the ligands, it is possible, in principle, to combine the therapeutic potential of metals with the multiple delivery of the various ligands, provided these latter are pharmacologically active molecules [6,20,21]. Specifically, it is the presence of the dimetallic core allowing the coordination of up to four releasable ligands. In this context, dimolybdenum (II,II) compounds -that are typically characterized by an unconventional multiple Mo-Mo bond [22] - have been far less investigated than di-Ru, Rh, and Os complexes, especially the solution stability, activation profile and the related biological activity. Nevertheless, some evidence of the anti-inflammatory, anticancer, and antibacterial profile of Mo-based complexes has been reported [23–26]. Accordingly, with the aim to start filling this gap, we report here the synthesis, multi-technique chemico-physical characterization and the first biological assessment of a series of dimolybdenum (II,II) compounds where the Mo-Mo core is coordinated with four NSAID ligands, namely, ibuprofen, naproxen, aspirin and indomethacin. These latter were selected because they are widely employed as ligands, owing to the presence of the carboxylate moiety capable of coordination towards the metal centres [3,27,28]. The resulting compounds can couple the well-known properties of NSAIDs -i.e. anti-inflammatory, antithrombotic, the ability to reduce radicals, to induce apoptosis and to alter the membrane function- with the medicinal properties of the selected metals [27–29].

2. Results and discussion

2.1. Synthesis and characterization

In order to synthesize the dimolybdenum (II) carboxylate paddlewheel complexes of the general formula $Mo_2(\mu\text{-}O_2CR)_4$, some widely used starting materials are the hexacarbonyl complex $[Mo(CO)_6]$ [30,31] or the tetraacetate complex $[Mo_2(OAc)_4]$ [22,32]. The use of $K_4[Mo_2Cl_8]$ is also reported [33]. In this work, instead, the compound $(NH_4)_5[Mo_2Cl_9]\cdot H_2O$ (pentaammonium nonachlorodimolybdenum monohydrate) was effectively employed as precursor. $(NH_4)_5[Mo_2Cl_9]\cdot H_2O$ was obtained as a violet powder in high yields (~80%), following the procedure reported by Cotton [34]. The synthesis is fast and simple and requires treating $[Mo_2(OAc)_4]$ with concentrated HCl (37%) in the presence of NH_4Cl for 1 h. This compound has been usually used for the synthesis of dimolybdenum complexes $Mo_2Cl_4L_4$ or $Mo_2Cl_4(LL)_2$ (LL = bidentate ligand) [35,36] but it proved to be an ideal starting material for the synthesis of $Mo_2(\mu\text{-}O_2CR)_4$ paddlewheel complexes [37,38]. In fact, attempts to synthesize these compounds by carboxylate exchange reaction, starting from $[Mo_2(OAc)_4]$ in THF, failed in affording the desired products. Brown to dark green powders were obtained, which showed only signals belonging to the uncoordinated ligand in the ^1H NMR spectrum. The reaction of $(NH_4)_5[Mo_2Cl_9]\cdot H_2O$ with the NSAIDs (Fig. 1), instead, was rapid and occurred at room temperature. The yellow-orange solids started precipitating from the solution right after the addition of the ligand, and after a few hours of stirring, they were collected in good yields (60–70%) by filtering the solution.

The driving force of the synthetic reaction is likely the formation of the insoluble complexes together with a significant entropy effect deriving from the change in the total number of molecular species (i.e. the replacement of eight chloride ligands with four bidentate ligands). Next, compounds were characterized via NMR and IR spectroscopy. In the ^1H NMR spectra (Figs. S1-S4), the coordination of the NSAID molecules can be confirmed by the presence of a single set of resonances, which are generally downfield shifted, compared to the corresponding free ligand. In particular, the peaks, accounting for the vicinal protons of the carboxylate group, are significantly deshielded (0.5–0.6 ppm) with respect to the uncoordinated NSAID. This perfectly confirms the coordination of the carboxylate to the dimolybdenum core. The HR-ESI-MS analysis further confirmed the obtainment of the desired products (see the experimental section and supporting material for both NMR and mass spectra). In Fig. 2, the IR spectra of NSAIDs and corresponding $Mo_2(NSAID)_4$ complexes **1**–**4** are displayed in the 1850–1110 cm^{-1} region, which resulted to be the most informative. The comparative and comprehensive investigation of the IR profiles (see below) allowed to infer the formation of dimolybdenum complexes (Table 1).

Specific spectral details of each system are reported below.

(1) $Mo_2(ibuprofen)_4$. The complex formation is proved by the absence in the complex spectrum of the following bands, all attributable to the vibrational modes of the carboxylic group: 1711 cm^{-1} (ν C═O), 1320 cm^{-1} (δ C-OH), 1229 cm^{-1} and 1183 cm^{-1} (ν C-OH) [39,40]. Moreover, it is noteworthy that, in the spectrum of the complex, the two bands at 1498 cm^{-1} and 1407 cm^{-1} appeared attributable to asymmetric and symmetric ν COO, and the one at 1289 cm^{-1} to ν O-C-O in the carboxylate group [41].

(2) $Mo_2(naproxen)_4$. The lack in the complex spectrum of the band at 1726 cm^{-1}, assigned to the ν C═O in the carboxylic acid moiety, gives evidence of the formation of the complex [39,42]. This is also confirmed

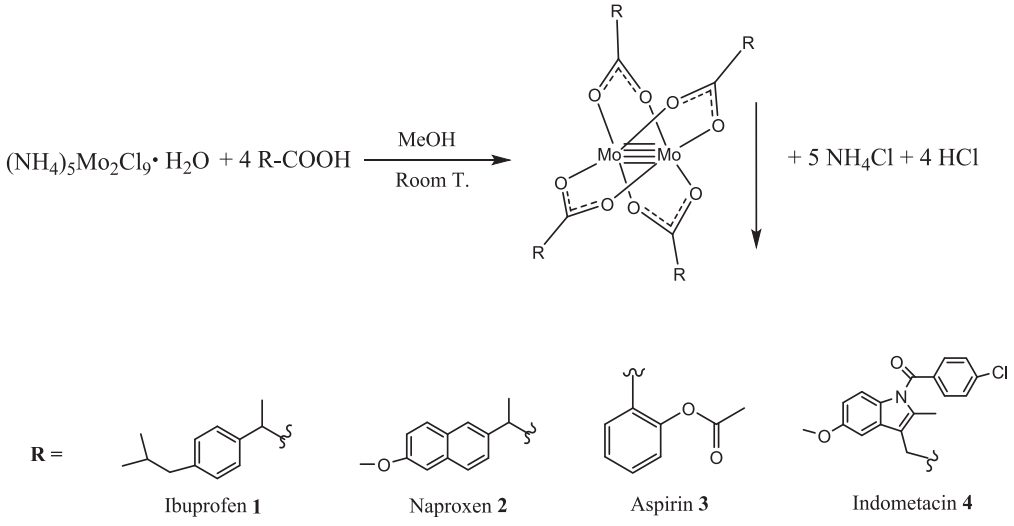

Fig. 1. Reaction route for the preparation of the $Mo_2(NSAID)_4$ complexes.

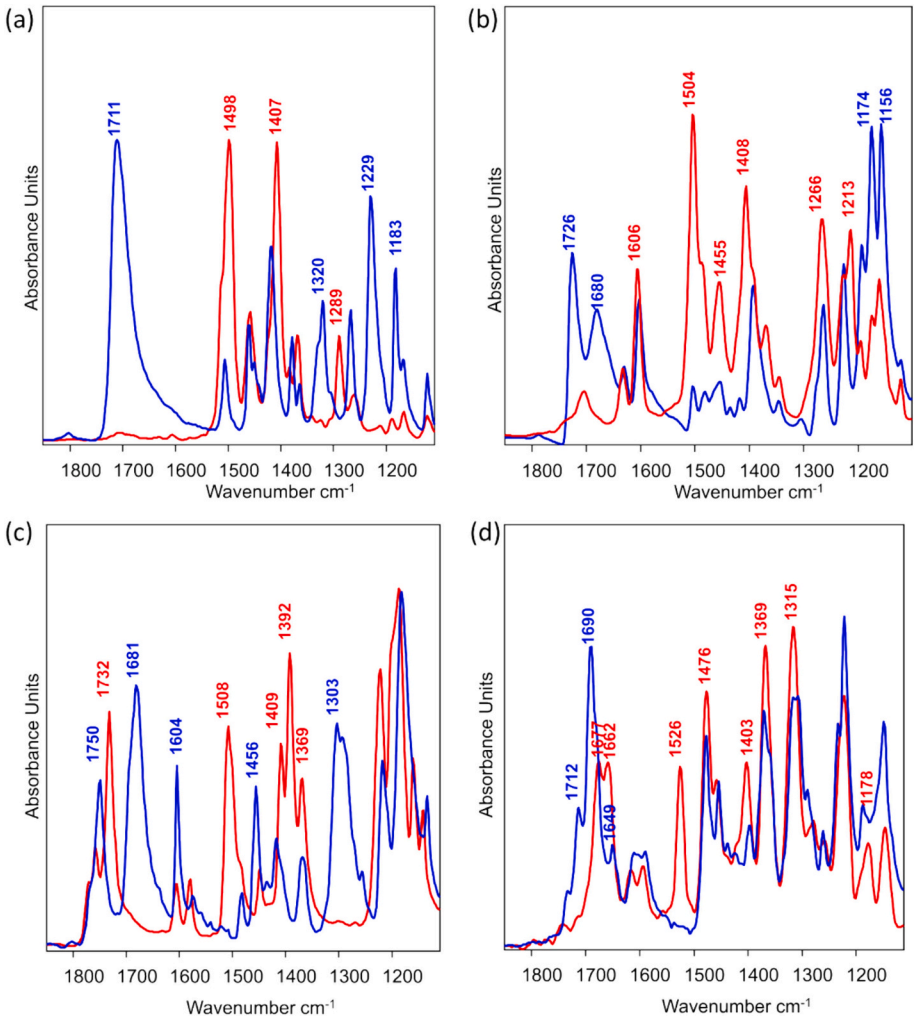

Fig. 2. IR spectra of: (a) ibuprofen (blue) and Mo_2(ibuprofen)$_4$ (red), (b) naproxen (blue) and Mo_2(naproxen)$_4$ (red), (c) aspirin (blue) and Mo_2(aspirin)$_4$ (red), and (d) indomethacin (blue) and Mo_2(indomethacin)$_4$ (red). Spectra are displayed in the 1850–1110 cm^{-1} range. The most informative peaks are labelled. (For interpretation of the references to colour in this figure legend, the reader is referred to the web version of this article.)

Table 1
Comparison of selected IR bands.

Compound	IR: ν/cm^{-1}		
	ν_{asym} (CO_2)	ν_{sym}(CO_2)	Other bands
1	1498	1407	–
2	1504	1408	–
3	1508	1392	1732 (ν C=O_{ester}) 1604(ν C=$C_{phenyl\ ring}$)
4	1526	1403	1677 (ν C=O_{amide})

by the appearance in the complex spectrum of the bands at 1504 cm^{-1} and 1408 cm^{-1}, attributable to the asymmetric and symmetric ν COO, and 1213 cm^{-1} due to ν C-O in the carboxylate group [41].

(3) Mo_2(aspirin)$_4$. The formation of the complex is clearly evidenced by the absence in the complex spectrum of the bands at 1681 cm^{-1} and 1303 cm^{-1}, assigned respectively to ν C=O and δ C-OH vibrations in the carboxylic acid moiety [39]. This hypothesis is also confirmed by the appearance of the bands at 1508 cm^{-1} and 1392 cm^{-1} in the complex spectrum, attributable to asymmetric and symmetric ν COO in the carboxylate group [41]. Moreover, in the same spectrum, the ν C=O ester band shifted from 1750 cm^{-1} to 1732 cm^{-1}, and the band at 1604 cm^{-1}, assigned to ν C=C phenyl ring, decreased in intensity [41].

(4) Mo_2(indomethacin)$_4$. Also in this case, the complex formation is confirmed by the disappearance in the complex spectrum of the band at 1712 cm^{-1} (ν C=O in the carboxylic acid moiety) [43] together with the concurrent appearance of the bands at 1526 cm^{-1} and 1403 cm^{-1}, attributable respectively to the asymmetric and symmetric ν COO in the carboxylate group [40,41]. Moreover, it is noteworthy that we observe a shift from 1690 cm^{-1} in the indomethacin spectrum to 1677 cm^{-1} in the complex spectrum (ν C=O amide) [43].

Elemental analysis of the four complexes was also performed. The results are different based on the experimental conditions. Indeed, when samples' preparation was done under inert atmosphere, the calculated composition matches the expected one for all compounds. Conversely, when the same analysis was done exposing **1**–**4** to the air, they undergo partial conversion into the corresponding oxides (Table S1). This could be explained by the poor air stability of the complexes. In fact, in this latter case the solids were exposed to air during the weighing operations prior to the measurement. In other words, despite the obtainment of the pure complexes (as attested by the independent analysis), the degradation occurred before the analysis itself, being this aspect in accordance with the nature of other dimolybdenum carboxylate paddlewheel compounds, vide infra. However, even in this latter case the CHN analysis is reliable because of the absence of the N and, thus, of the counterion NH_4^+ that belongs to the precursor (except for compound **4** bearing the indomethacin ligand; for which the experimentally determined % of N is in perfect agreement with the theoretical one).

All the compounds are nearly insoluble in alcohols, water, and halogenated solvents and moderately soluble in acetone. The solubility is good in DMSO and DMF. They are all air sensitive, and the solids start to discolour after hours upon air exposure. However, this was not surprising, since the susceptibility to oxidation of the dimolybdenum carboxylate paddlewheel complexes is well known [31,44,45]. When dissolved in DMSO, the NSAID ligands are released over time. The solutions of complexes **1** and **2** turned from yellow to green-blue after 24 h of exposure to air, while solutions of **3** and **4** required longer times (days) for the same change in the colour. The different stability in DMSO was then studied comparatively using ^{1}H NMR spectroscopy. The release of ligands was monitored at different time intervals (2, 4, and 24 h) and the degradation percentage was calculated (Table 2).

The complexes' stability in DMSO solution greatly depended on the ligands coordinated to the dimolybdenum core. Complexes **1** and **2** resulted to be less stable, degrading almost completely in 24 h, while complex **3**, with aspirin as ligand, turned out to be the most stable.

For longer incubation times (48–72 h) all the compounds resulted almost completely degraded under the applied experimental conditions (data not shown).

2.2. Theoretical calculations

The computational assessment of the stability as well as the characterization of the reactivity of dimolybdenum (II) complexes were carried comparatively for convenience. Hence, the structural and energy trends, calculated on the dimolybdenum (II) complexes, were compared with the same data retrieved on analogous diruthenium (II) complexes. Such an approach was expected to improve the reliability of the computational outcomes. For this purpose, the geometrical and electronic structures of dimolybdenum complexes **1**–**4** were calculated and compared with the analogous diruthenium complexes, respectively labelled **1′**-**4′**. The geometries of **1**–**4** and **1′**-**4′** paddlewheel complexes (Fig. 3, Figs. S9-S12) were optimized by DFT approaches (see computational details). The most significant geometrical parameters, retrieved from the DFT structures, are presented in Table 3. We noticed that the bridging carboxylate fits better the Ru-Ru bond (2.27–2.28 Å) than the shorter Mo-Mo bond (2.04–2.05 Å). Indeed, the O···O distance in the unbound carboxylate ligand was found to be 2.24 Å in all examined NSAIDs, thus suggesting that the intermetallic distance in diruthenium compared to the dimolybdenum scaffold complexes may enhance the μ-coordination. The higher strength of Ru-O compared to Mo-O bond was also corroborated by the corresponding bond distances of 2.02–2.05 and 2.11–2.13 Å, respectively (Table 3).

Such evidence suggests that the stability of the dimetallic scaffold, represented by the strength of the M-M bond, might be inversely correlated to the stability of the carboxylate coordination. As previously reported [46,47], the occupation of the axial position of bimetallic paddlewheel complexes by solvent molecule may induce destabilization, hence, the possible coordination of DMSO at axial position of dimolybdenum and diruthenium complexes was computationally assessed. Interestingly, we found that DMSO cannot occupy the axial positions in dimolybdenum complexes in solution, even though its O-coordination at the Mo_2 tetracarboxylate complexes has been evidenced in the crystalline phase [48]. On the other hand, the axial coordination of DMSO on the diruthenium complexes, as expected, elongates the intermetallic bond by 0.07–0.12 Å as well as the Ru-Cl bond by 0.04 Å (Table 3). These data indicate that the stability of dimolybdenum compared to the analogous diruthenium complexes is not directly influenced by the coordination of solvent molecules, but we hypothesize it is more likely ascribable to an intrinsically weaker carboxylate coordination in the former complexes. In order to assess the strength of the bridging ligand coordination, we have calculated the metal-carboxylate bond breaking energies, i.e. the energy amount required for the breaking of the μ-coordination of one carboxylate ligand without taking into account the further relaxation of the detached fragments, for the studied dimolybdenum and diruthenium complexes. The bond breaking energies for the diruthenium complexes are ~20 kcal/mol higher than the corresponding values for the dimolybdenum complexes (Table 3), while the axial coordination of DMSO affects only marginally the bond breaking energies of the bridging ligands in either dimolybdenum or diruthenium complexes. To better characterize the reactivity of compounds **1**–**4** and **1′**-**4′**, with a special focus on the stability of the respective paddlewheel architectures, the charge distribution and the orbital interactions underlining the coordination of one carboxylate moiety to the bimetallic center were analysed on the reduced model complexes $Mo_2(CH_3COO)_4$ and $ClRu_2(CH_3COO)_4$, which are though representative of the metal-carboxylate interaction detectable in the **1**–**4** complexes.

NBO analyses allowed to compute the charge distribution in both $Mo_2(CH_3COO)_4$ and $ClRu_2(CH_3COO)_4$ complexes, as well as the spin

Table 2
Degradation percentages of the complexes at increasing time intervals in DMSO-d_6. Red numbers correspond to complexes.

Time (h)	Degradation Percentage			
	1	2	3	4
2	16%	15%	15%	19%
4	25%	42%	23%	26%
24	84%	84%	44%	59%

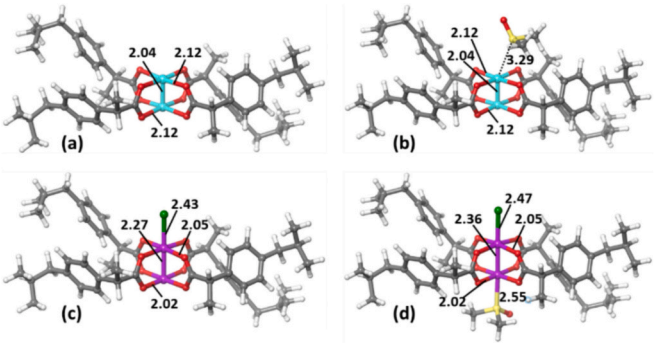

Fig. 3. Optimized structures of complexes (a) **1**, (b) **1**-DMSO, (c) **1′**, and (d) **1′**-DMSO with the indicated M-M, M-O, M-Cl, and M-S distances in angstrom. The indicated M-O distances are the average values for each metal center. Colour scheme: Ru (plum), Mo (cyan), Cl (green), S (yellow), O (red), C(grey), H (white). (For interpretation of the references to colour in this figure legend, the reader is referred to the web version of this article.)

Table 3
Calculated geometrical parameters (Å)and bond breaking energies (kcal/mol) of dimolybdenum(II) **1**–**4** and diruthenium(II) **1′**-**4′** complexes, as well as their corresponding adducts with one DMSO ligand.

Complex	Distance					Bond breaking energy
	M-M	M1-O	M1-Cl	M2-O	M2-S	
1	2.04	2.12	n/a	2.12	n/a	83.3
1-DMSO	2.04	2.12	n/a	2.12	3.29	83.7
1′	2.27	2.05	2.43	2.02	n/a	103.8
1′-DMSO	2.36	2.05	2.47	2.02	2.55	106.3
2	2.04	2.12	n/a	2.13	n/a	88.0
2-DMSO	2.04	2.12	n/a	2.12	3.25	90.3
2′	2.28	2.05	2.43	2.02	n/a	109.0
2′-DMSO	2.36	2.05	2.47	2.02	2.55	112.0
3	2.05	2.11	n/a	2.11	n/a	78.5
3-DMSO	2.05	2.12	n/a	2.11	3.78	80.7
3′	2.28	2.05	2.42	2.02	n/a	99.7
3′-DMSO	2.39	2.05	2.46	2.03	2.51	100.3
4	2.04	2.11	n/a	2.13	n/a	98.8
4-DMSO	2.04	2.13	n/a	2.13	3.26	97.8
4′	2.27	2.05	2.42	2.02	n/a	119.2
4′-DMSO	2.34	2.05	2.46	2.02	2.61	114.7

density on the latter. As expected, compared to the formal charge +4 and +5 of the Mo_2 and Ru_2 centers, respectively, calculations showed much lower values, i.e. +1.717 and +2.084, consistently with the negative charge transfer accompanying the coordination of the four carboxylate units (Table 4). Notably, such a negative charge transfer was slightly larger in the Ru_2 complex as displayed by the lower negative charge residual on the four carboxylate moieties (Table 4). The spin density on the Ru_2 scaffold confirmed that almost all the three unpaired electrons in this quadruplet complex are localized on the bimetallic moiety and (by a small fraction) on the axial Cl atom. These results provided for a preliminary indication of a more effective σ coordination of the carboxylate groups on the Ru_2 compared to the Mo_2 scaffold. Moreover, the natural electron configuration (NEC) data confirmed that a higher amount of negative charge is transferred to the Ru_2 scaffold; indeed, while the NEC on one Mo center was computed to be 4.66, i.e. +0.66 over the formal d^4 character, the NEC on one Ru center was 6.60 which is +1.1 over the formal $d^{5.5}$ character (Table 4).

The correlation diagrams depicting the relevant combinations between one carboxylate moiety and the bimetallic scaffold in $Mo_2(CH_3COO)_4$ and $ClRu_2(CH_3COO)_4$ complexes were reported (Fig. 4). The μ-coordination of carboxylate to the $[Mo_2(CH_3COO)_3]^+$ metal fragment can be described by the combination of doubly occupied orbitals of carboxylate with the low-energy empty orbitals on the bimetallic moiety. The carboxylate moiety presents four electron pairs available to the metal, corresponding to its HOMO-3 to HOMO orbitals, with the HOMO and HOMO-2 describing the two electron pairs amenable to σ combinations and the HOMO-1 and HOMO-3 amenable to π combinations (Fig. S15). On the other hand, the $[Mo_2(CH_3COO)_3]^+$ metal fragment presents two empty orbitals, i.e. LUMO and LUMO+4, shaped to combine with the σ lone pairs of carboxylate, and two orbitals, i.e. HOMO and LUMO+1, amenable to π combinations (Fig. 4). We detected two bonding σ combinations, and one π combination with a bonding character. The π combination involving the HOMO of the $[Mo_2(CH_3COO)_3]^+$ metal fragment and the HOMO-3 of the carboxylate moiety as no bonding character, but concurs to determine the HOMO of the whole complex (Fig. 4). Above all, the coordination of one acetate to the $[Mo_2(CH_3COO)_3]^+$ metal fragment involves two σ and one π electron pairs. The analysis of the orbital interactions between the $[ClRu_2(CH_3COO)_3]^+$ metal fragment and one acetate yielded a slightly different picture because of the d^6d^5 character of the Ru_2 bimetallic center, and because of the axial chloro ligand that contributes to the shape and the energy of the frontier orbitals on the metal fragment (Fig. 5). In particular, we detected three orbitals on the Ru_2 moiety, i.e. LUMO+1, LUMO+2, and LUMO+3, amenable to combine with the carboxylate electron pairs. In this case, beside the involvement of the HOMO and HOMO-2 electron pairs, as also detected in the Mo_2-carboxylate analysis, the electron pair on the HOMO-4 of acetate was found to contribute to σ combination, thus conferring the Ru_2-carboxylate bonding compared to the Mo_2-carboxylate a higher σ character. On the other hand, only two orbitals-four electrons combinations were retrieved in the picture of Ru_2-carboxylate π interactions (Fig. 5). Hence, although three electron pairs are involved in both bimetallic-carboxylate interactions, the coordination at Ru_2 was found to have a higher σ character compared to the coordination at Mo_2, in agreement with the higher Ru_2-carboxylate dissociation energies calculated in the **1**–**4** complexes (Table 3).

Table 4
NBO analyses of $Mo_2(CH_3COO)_4$ and $ClRu_2(CH_3COO)_4$ complexes reporting the charge per molecular fragment (basin), the spin density (spin), and the natural electron configuration (NEC).

Complex	Basin	Charge	Spin	NEC (valence)
$Mo_2(CH_3COO)_4$	Mo_2	+1.72	n/a	Mo: $5s^{0.23}4d^{4.66}5p^{0.08}5d^{0.03}$
	$(CH_3COO^-)_4$	−1.72	n/a	O: $2s^{1.68}2p^{4.98}3p^{0.01}$
$ClRu_2(CH_3COO)_4$	Ru_2	+2.08	2.60	Ru: $5s^{0.30}4d^{6.60}5p^{0.01}5d^{0.04}$
	$(CH_3COO^-)_4$	−1.65	0.23.	O: $2s^{1.72}2p^{4.98}3p^{0.01}$
	Cl	−0.43	0.16	Cl: $3s^{1.96}3p^{5.47}$

The analysis of the orbital interactions between the bimetallic fragment and the equatorial carboxylate ligand also spotlighted the composition of the paddlewheel complexes frontier orbitals, and provided a preliminary insight of the reactivity of Ru_2 and Mo_2 complexes. Indeed, by taking the complex **1** and **1′** as exemplificative, both bimetallic fragments were featured by low energy lying empty orbitals expanded on the axial vacant position which are thus suitable of nucleophilic attacks (Fig. 5). On the other hand, the presence of two vacant axial positions on the Mo_2 complex **1** may be an explanation of its higher reactivity compared to **1′** with only one axial site available. The LUMO+1 of complex **1′** was also found to lay at a lower energy, thus explaining the formation of the adduct with DMSO. It is also worth noticing the higher participation of the π systems on the phenyl rings of **1** to either LUMO+1 and LUMO+2 orbitals (Fig. 5), which probably reflects the partial π bonding character of the Mo_2-carboxylate interaction. Conversely, the LUMO+1 of the **1′** displayed no contribution of the phenyl orbitals (Fig. 5).

Further structural signatures of $Mo_2(NSAID)_4$ complexes were investigated by comparing the experimental and calculated IR spectra of the exemplificative complex **1**. We focused on the range of low vibrational frequencies expected to reflect normal modes with high contributions of the metal scaffold.

The calculated and experimental IR spectra of complex **1** were found to be rather comparable (Fig. S13 and S14). Indeed, for the most intensive three bands around 1500 cm^{-1}, i.e. asymmetric C-O stretching, symmetric C-O stretching, and H–C–H bending at 1528, 1443, and 1400 cm^{-1}, respectively, the corresponding experimental signals, 1500, 1400, and 1360 cm^{-1}, respectively, were assigned (Fig. S13).

Therefore, the C_{Ar}–C_{Ar} stretching signal, computationally located at 1498 cm^{-1} and overwhelmed by the much more intensive asymmetric C-O stretching signals, can be putatively assigned to the experimental peak at 1470 cm^{-1} (Fig. S13). On this basis, we tentatively hypothesized that each experimental band is approximately red-shifted by, on average, 30 cm^{-1} with respect to the corresponding calculated signal. Such a deviation can be ascribed to the fact that the solid-state packing of the $Mo_2(ibuprofen)_4$ units affects the experimental IR spectrum, whereas such an effect is totally neglected in the calculated spectrum. It is also worth noticing that the IR spectrum calculated in DMSO (implicit solvation) compared to the one calculated in gas phase was found in slightly higher agreement with the experimental data; these data may indicate that implicit solvation could partially account for the interunit interactions displayed in the solid phase.

The calculated and experimental IR spectra in the lower energy region, i.e. 200–1000 cm^{-1}, showed in both cases 12 bands that we tentatively reputed assignable, based on the above-mentioned average 30 cm^{-1} red-shift (Fig. S14). The analysis of the normal modes of the calculated bands indicated that most of these signals are characterized by out-of-plane (oop) bending contributions. On the other hand, the peaks in the 413–660 cm^{-1} range (calculated spectrum) were all characterized by a mixture of oop bending and asynchronous Mo-O stretching contributions; the synchronous Mo-O stretching was also found to be mixed with oop bending modes but located at 405 cm^{-1} (Fig. S14).

The mixture of Mo-O stretching, clearly specific of the bimetallic moiety, and oop bending modes, mostly ascribable to internal NSAID modes, suggest that the ensemble of IR absorbance bands in the low frequency region can be used as a signature of the $Mo_2(NSAID)_4$ structure.

2.3. Biological studies

Next, to gather the proof of concept that disassembling and subsequent release of the active ligands occurred also in a biological

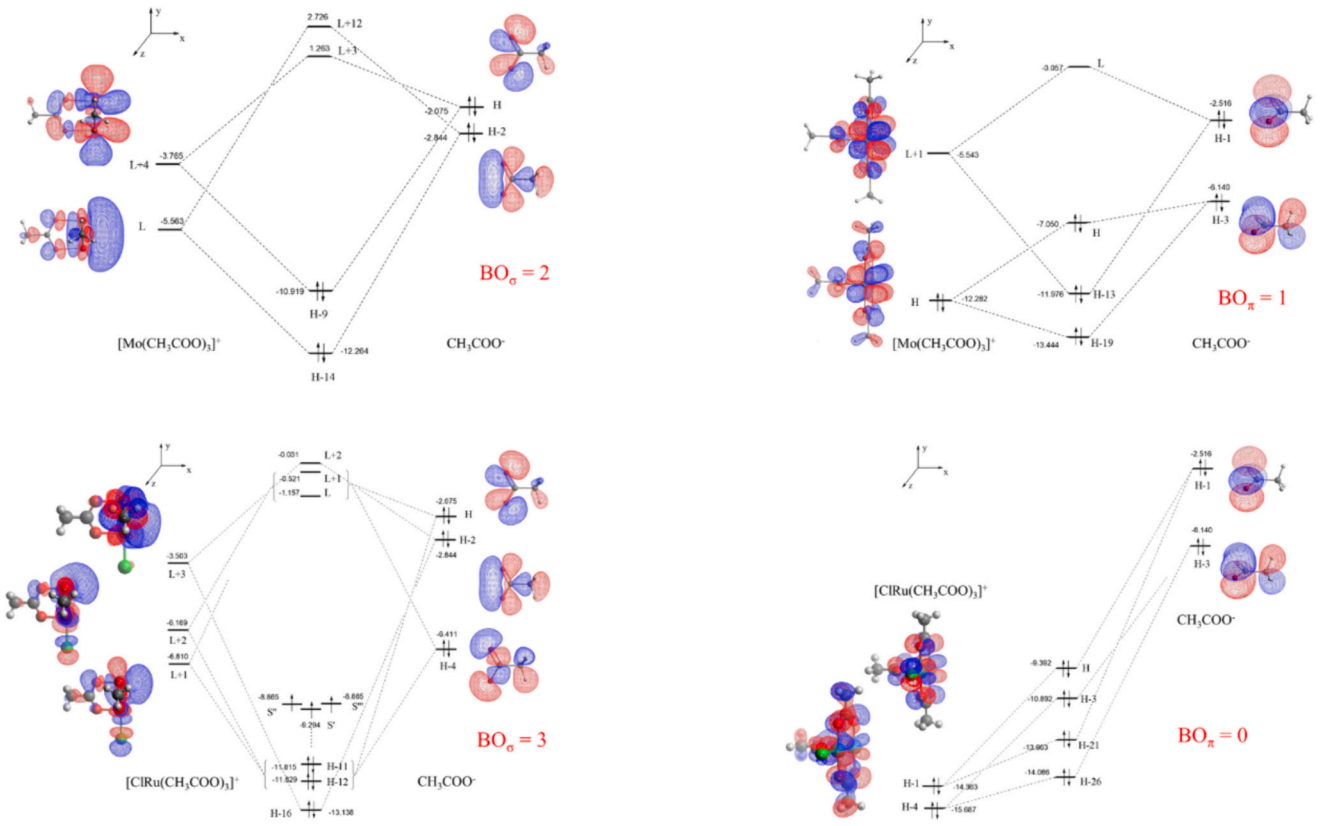

Fig. 4. Orbital diagrams of the bimetallic–carboxylate interaction σ (left) and π (right) in $Mo_2(CH_3COO)_4$ (up) and $ClRu_2(CH_3COO)_4$ (down) complexes. The metal-metal bond is alined along the z axis, while the acetate fragment lays on the xz plane. Orbital energy values are reported in hartree. The bond order (BO) computed on each diagram is also reported.

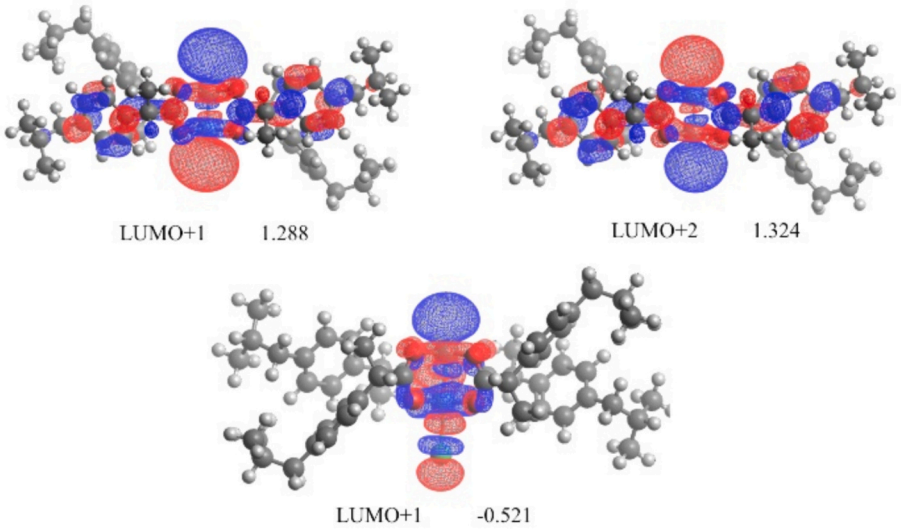

Fig. 5. Rendition of the LUMO+1 and LUMO+2 of complex **1** (up), and of the LUMO+1 of complex **1′** (down).

environment, the cytotoxic effects of complexes **1** (the less stable) and **3** (the most stable complex) on a panel of human cancer cell lines were investigated and compared to ibuprofen and aspirin (Table 5). Specifically, the effects on human breast adenocarcinoma cells (MDA-MB-231), human type II alveolar epithelial cells (A549), and human glioblastoma cells (U87MG) were assessed using the MTS assay. Both derivative treatments (10 μM – 1 mM) for 72 h caused a decrease in proliferation yielding IC_{50} values in the high micromolar range.

Though **1**–**4** undergo degradation in shorter times, these experiments were conducted at the 72 h time point to account for possible biological effects triggered by the drugs, that may occur later. Ibuprofen alone was able to slightly decrease the cell viability in a dose-dependent manner in all the cell lines, in accordance with literature data [49–51]. Interestingly, the IC_{50} values for **1** on the A549 and U87MG were lower with respect to ibuprofen. Based on the results, we can assume that upon degradation/activation of **1** in the biological milieu, the molybdenum derived species (including the molybdenum oxide ones) can positively impact the overall biological observed effect [24]. Aspirin was able to

Table 5
IC_{50}[a] values (1, 3, and Ibuprofen) or the maximum percentage of inhibition at 1 mM (Aspirin) on MDA-MB231, A549, and U87MG cells.

Compound	MDA-MB-231	A549	U87MG
1	1103 ± 490	617 ± 150	684 ± 221
3	601 ± 103	891 ± 220	374 ± 87
Ibuprofen	963 ± 152	1043 ± 10	952 ± 204
Aspirin	32.1 ± 8.9%	n.a.	46.1 ± 14.0%

[a] IC_{50} values (μM) were reported as mean ± SEM of three different experiments. The value of the SEMs of 1 and 3 reflects their high reactivity and solubility profiles; however, the trend can be clearly outlined. When an IC_{50} value cannot be extrapolated, the decrease of cell viability percentage at 1 mM was introduced. (n.a. = non-active).

decrease the cell viability only when a 1 mM concentration was applied. Its derivative **3** produced a higher effect in all the cell lines. The treatment with dimolybdenum acetate $[Mo_2(OAc)_4]$ did not affect cell proliferation at all the used concentrations (data not shown). Altogether, thought the effects occurred at relatively high doses, yet this result is relevant because highlights that, from a mechanistic point of view, derivatives **1** and **3** can release their constituents in the biological environment potentially promoting pharmacological effects.

Among the two compounds, **3** was not only the most stable, but on average, also the most active. Accordingly, we selected it to assess whether this compound could perform anti-inflammatory effects [52]. As the compound releases aspirin, we investigated whether it could exert anti-inflammatory action in U87MG cells. Cells were treated with lipopolysaccharide (LPS, 1 μg/mL) to increase basal inflammatory levels and then were treated with **3** (final concentration 250 μM) at a concentration near the IC_{50} value or aspirin (final concentration 1 mM) for 48 h. This aspirin concentration was four times higher with respect to the complex to maintain the amount of ligand that could be released by the 250 μM concentration of the compound. The gene expression of the pro-inflammatory cytokine interleukin-6 (IL-6), the enzymes cyclooxygenase-2 (COX-2), which is the main target of aspirin, and the nuclear factor kappa-light-chain-enhancer of activated B cells (NF-kB), which plays a pivotal role in orchestrating inflammatory response, was investigated (Fig. 6). As expected, the LPS alone was able to significantly increase the expression of all the investigated genes. The complex **3** treatment significantly counteracted the increase of IL-6 and COX-2 expression, but not the NF-kB, while the aspirin alone reduced also the NF-kB increase. Altogether, these data suggest that **3** can exert an anti-inflammatory effect, demonstrating also in this case its ability to release the aspirin ligands. However, the same amount of aspirin produces a more pronounced effect, indicating that the rate of disassembling of compound and thus the rate of ligands release may impact the overall pharmacological profile.

3. Conclusions

In this paper, we report on the synthesis and multi-technique characterization of a panel of compounds featured by the presence of a bimetallic Mo-Mo core and NSAID ligands, ibuprofen, naproxen, aspirin, and indomethacin. The resulting paddlewheel complexes were then studied comparatively for their reactivity. The activation profiles in solution revealed **1** and **2** as endowed with the lowest stability after 24 h in solution, while **3** was the most stable. The reasons for the difference in the solution behaviour and activation of the complexes were next theoretically investigated. The computational assessment of the stability of $Mo_2(NSAID)_4$ complexes yielded an insight into the chemistry that may operate the dismantling of the paddlewheel structure. Indeed, the Mo_2 scaffold was found to be characterized by a lower stability and higher reactivity compared to its $[Ru_2(NSAID)_4]^+$ counterpart, presumably ascribable to the less effective μ-coordination of the carboxylate group at the Mo_2 moiety. The calculation of the IR spectra of $Mo_2(ibu)_4$ allowed us to assign most of the experimentally detected bands and to spotlight the region of the low energy modes, in particular the 413–660 cm^{-1} region, as being potentially a signature of these complexes. The experiments against a panel of cancer cells highlight that compounds are on average scarcely cytotoxic, inducing cell death effects only for concentration > 500 μM. However, it should be noticed that **1** and **3** resulted more active than ibuprofen and aspirin, respectively, this evidence supporting some role of Mo in inducing the observed activity. Next, the pilot study on compound **3** -i.e. the complex that previously determined the greatest cellular effect- was carried out to assess its anti-inflammatory profile, confirming again the capability to disassemble releasing the functional anti-inflammatory drug in the biological milieu. Considering the unconventional paddlewheel shape and the possibility of multiple coordination of biologically active agents acting as ligands towards the bimetallic core, these compounds potentially represent valuable chemical scaffolds for biological applications. Importantly, our investigation also allowed to delineate some relevant aspects of the reactivity and activation pathways of this family of compounds. This offers a tool for controlling and tuning their reactivity and activation -specifically, it seems crucial the balance between stability and the rate of ligands' release- and, based on these findings, for the design of more effective bimetallic core-bearing paddlewheel complexes.

3.1. Experimental section

All solvents and reagents were purchased from Sigma-Aldrich and used without further purification. The synthesis of $(NH_4)_5[Mo_2Cl_9]\cdot H_2O$ was carried out, according to a known procedure [34]. All reactions were performed under inert atmosphere (N_2) and the solvent used (MeOH) degassed with nitrogen for 30 min. Compounds were stored

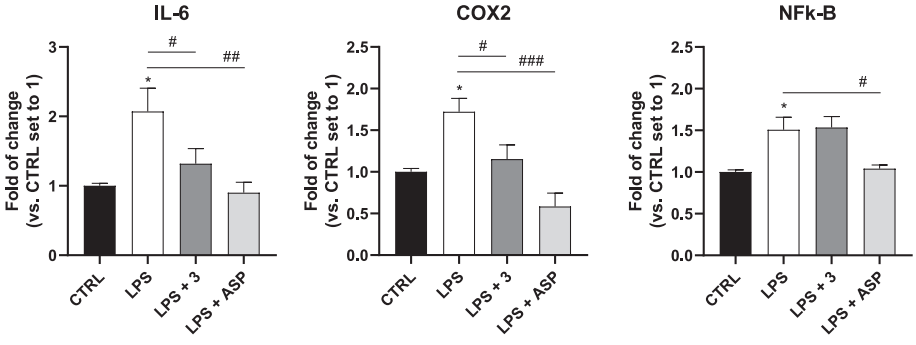

Fig. 6. Anti-inflammatory effects of **3** on glioblastoma cells. U87MG cells were treated with LPS (1 μg/mL) for 2 h and then **3** (250 μM) or aspirin (ASP, 1 mM) were added, and the real-time PCR was performed after 48 h for IL-6, COX2, and NF-kB. Data are expressed as the fold of change versus control set to 1 and are the mean values ± SEM of three different independent experiments performed in duplicate. The significance of the differences was determined by one-way ANOVA, followed by Bonferroni's post hoc test: *$p < 0.05$ vs CTRL; # $p < 0.05$, ## $p < 0.01$, ### $p < 0.001$, vs LPS.

under inert atmosphere at −20 °C. ^{1}H NMR and ^{13}C{^{1}H}-NMR spectra were recorded at 293 K on a Bruker Avance II 400 MHz, chemical shifts (expressed in parts per million, ppm) were referenced to solvent residual peaks. For both characterization and stability experiments (see below) anhydrous DMSO, 99.9 atom % D, code: 570672, was used. The water content was ≤50.0 ppm. The NMR tube for each complex was prepared under inert atmosphere (anhydrous N_2). The tubes were sealed under the same inert atmosphere also using parafilm. The spectra were processed using the MestreNova software. Elemental analysis (C,H,N) was accomplished through VarioMICRO elemental analyser. ESI mass spectra were recorded using an Orbitrap high-resolution mass spectrometer (Thermo, San Jose, CA, USA), equipped with HESI source. The working conditions were as follows: positive polarity, spray voltage 3.5 kV, capillary temperature 300 °C, and S-lens RF level 55. The sheath and the auxiliary gases were set at 20 and 3 (arbitrary units), respectively. Complexes were solubilized in LC-grade anhydrous acetonitrile, just before the analysis. The working conditions were as follows: positive polarity, Spray voltage 3.4 kV, capillary temperature 290 °C, S-lens RF level 50.

Sheath gas 24, auxiliary gas 5 (arbitrary units) respectively. Attenuated Total Reflectance – Fourier Transform Infrared (ATR-FTIR) analysis was performed at the Advanced research Laboratory, Polytechnic University of Marche. The IR spectra of $Mo_2(NSAID)_4$ together with the NSAIDs alone were collected in the reflectance mode by an INVENIO FTIR Spectrometer (Bruker Optics, Ettlingen, Germany), coupled with a Platinum ATR (Attenuated Total Reflectance) accessory, mounting a diamond crystal, and equipped with a DTGS (deuterated triglycine sulphate) detector. For each compound, five spectra were recorded in the 4000–400 cm^{-1} spectral range (512 scans, spectral resolution 4 cm^{-1}). Before each sample measurement, a background spectrum was collected with the same set-up conditions on the clean diamond crystal. Raw IR spectra were then absorbance converted, 2-point baseline corrected (64 baseline points), and vector normalized (OPUS 7.5, Bruker Optics, Ettlingen, Germany). Finally, for each compound, the average spectrum was calculated.

3.2. Synthesis of the $Mo_2(NSAID)_4$ complexes

In a Schlenk flask containing $(NH_4)_5Mo_2Cl_9{\cdot}H_2O$ (100 mg, 0.16 mmol; 1 eq.), 3 mL of deaerated MeOH were added. The purple suspension was magnetically stirred for a few minutes and 0.8 mmol (5 eq.) of the desired NSAID ligand were then added. Upon the addition, the colour of the solution rapidly turns from purple to yellow-orange. After stirring for 2 h at room temperature, the precipitated solid was collected using vacuum filtration and washed with H_2O (10 mL) and MeOH (10 mL). The yellow-orange powders obtained were dried under vacuum for several hours over $CaCl_2$ and then collected. Fig. 1 summarizes the synthetic route used for the preparation of $Mo_2(NSAID)_4$ complexes.

Yields were the following: **1**) 68% **2**) 69% **3**) 58% **4**) 66%.

^{1}H NMR (400 MHz; DMSO-d_6): (**1**) 7.22 (d, J = 8.0 Hz, 2H, H arom.), 7.11 (d, J = 8.0 Hz, 2H, H arom.), 4.22 (q, J = 7.2 Hz, 1H, CH-COOH), 2.44 (d, J = 7.1 Hz, 2H, CH_2), 1.84 (oct., J = 6.9 Hz, 1H, CH), 1.58–1.42 (m, 3H, CH_3), 0.87 (d, J = 6.6 Hz, 6H, CH_3). (**2**) 7.74 (m, 2H, H arom.), 7.64 (d, J = 8.6 Hz, 1H, H arom.), 7.33 (dd, J = 8.5, 1.7 Hz, 1H, H arom.), 7.26 (d, J = 2.4 Hz, 1H, H arom.), 7.18–7.14 (m, 1H, H arom.), 4.33 (q, J = 7.0 Hz, 1H, CH-COOH), 3.87 (s, 3H, CH_3-O), 1.58 (d, J = 7.2 Hz, 3H, CH_3). (**3**) 8.17 (dd, J = 7.7, 1.7 Hz, 1H, H arom.), 7.61–7.56 (m, 1H, H arom.), 7.44 (td, J = 7.6, 1.2 Hz, 1H, H arom.), 7.23 (dd, J = 8.0, 1.1 Hz, 1H, H arom.), 2.16 (s, 3H, CH_3). (**4**) 7.66–7.61 (m, 4H, H arom.), 7.06 (d, J = 2.5 Hz, 1H, H arom.), 6.92–6.86 (m, 1H, H arom.), 6.76–6.71 (m, 1H, H arom.), 4.09 (s, 2H, CH_2), 3.76 (s, 3H, CH_3-O), 2.14 (s, 3H, CH_3).

^{13}C{^{1}H}-NMR (101 MHz; DMSO-d_6): (**1**) 184.47 (COOH), 140.70 (C arom.), 139.70 (C arom.), 129.41 (C arom.), 127.44 (C arom.), 47.20 (CH-COOH), 44.77 (CH_2), 30.14 (CH), 22.66 (CH_3), 20.77 (CH_3). (**2**) 184.48 (COOH), 157.58 (C arom.), 138.18 (C arom.), 133.62 (C arom.), 129.58 (C arom.), 128.92 (C arom.), 127.30 (C arom.), 126.88 (C arom.), 126.03 (C arom.), 119.15 (C arom.), 106.22 (C arom.), 55.63 (CH_3-O), 47.40 (CH-COOH), 20.34 (CH_3).

(**3**) 173.45 (COOH), 169.43 (-COO-CH_3), 149.80 (C arom.), 133.75 (C arom.), 131.74 (C arom.), 126.03 (C arom.), 124.00 (C arom.), 21.38 (CH_3). (**4**) 180.41 (COOH), 168.26 (-C=O), 156.03 (C arom.), 138.11 (C arom.), 135.63 (C arom.), 134.56 (C arom.), 131.62 (C arom.), 131.17(C arom.), 130.77 (C arom.), 129.54 (C arom.), 115.10 (C arom.), 113.91 (C arom.), 111.78 (C arom.), 102.40 (C arom.), 55.82 (CH_3-O), 32.36 (CH_2), 13.65 (CH_3).

IR (cm^{-1}): (**1**) 2952br; 2349br; 1498s; 1459 m; 1408s; 1369 m; 1289 m; 1262w; 1189w; 1167w; 1122w; 1069 m; 1021w; 894 m; 851 m; 800 m; 731 s; 695 m; 609 s; 551 s; 471 s; 434w. (**2**) 2972br; 1704w; 1633w; 1606 m; 1503s; 1455 m; 1406s; 1370w; 1345w; 1266s; 1214s; 1196w; 1174 m; 1161 m; 1122w; 1067 m; 103 s; 984w; 961w; 927 m; 892 m; 853 s; 814 s; 748 m; 712 m; 692 m; 619w; 566w; 547w; 523w; 473 s; 435 m. (**3**) 1758s; 1732s; 1606w; 1580w; 1508s; 1449w; 1409s; 1392s; 1370s; 1223s 1188s; 1160 m; 1143 m; 1095s; 1033w; 1014 m; 958w; 914 m; 877w; 849 m; 814 m; 789w; 753 s; 724w; 706 m; 677 s; 653 s; 623w; 588 m; 548 m; 496 s; 454 m; 433 m. (**4**) 3749w; 3735w; 3649w; 1676s; 1658s; 1616 m; 1594 m; 1525s; 1477s; 1458s; 1420w; 1403s 1369s; 1315s; 1281w; 1260w; 1219s; 1090s; 1071s; 1036 m; 1018 m; 928 m; 903w; 857 m; 835 m; 799 m; 776w; 755 s; 738w; 717w; 695w; 679w; 637w; 626w; 608w; 552w; 509w; 483w; 458w; 438w; 419w.

CHN: (**1**) $C_{52}H_{68}Mo_2O_8$; required: C = 61.66; H = 6.67; N = 0.00. Found: C = 61.60; H = 6.74; N = 0.00. (**2**) $C_{57}H_{55}Mo_2O_{12}$; required: C = 60.91; H = 4.93; N = 0.00. Found: C = 60.75; H = 4.98; N = 0.00. (**3**) $C_{36}H_{28}Mo_2O_{16}$; required: C = 47.59; H = 3.11; N = 0.00. Found: C = 47.30; H = 3.18; N = 0.00. (**4**) $C_{76}H_{60}Cl_4Mo_2N_4O_{16}$; required: C = 56.38; H = 3.74; N = 3.46. Found: C = 55.99; H = 3.63; N = 3.48.

HR-ESI-MS (**1**) m/z $[M]^+$ = 1014.30060 (theoretical: 1014.30155); (**2**) m/z $[M]^+$ = 1110.15686 (theoretical: 1110.15603) (**3**) m/z $[M]^+$ = 908.94861 (theoretical: 908.94884); (**4**) m/z $[M + H^+]^+$ = 1620.09558 (theoretical: 1620.09142).

See supporting material for spectra and isotope pattern simulation.

3.3. ^{1}H NMR stability studies

A few milligrams of the complexes (3–5 mg) were weighed and dissolved in 500 μL of DMSO-d_6 affording 5 ·10^{-3} M solutions. ^{1}H NMR spectra were then acquired at different time intervals (0, 2, 4 and 24 h) for each compound. The degradation percentage was calculated at each time interval as $(\frac{a}{a^*+a})$*100 where a stands for the integral value of the resonance peak of a hydrogen belonging to the free ligand, and a* to the integral value of the coordinated one (Figs. S5-S8). The values obtained were normalized with respect to the degradation percentages assessed at the zero time. Main Text Paragraph.

3.4. Computational details

The Gaussian 16 quantum chemistry package was employed for all computations [53]. All geometry optimizations were performed by using the hybrid functional ωB97XD [54] with the basis set def2SVP [55,56] and implicit solvation (vide infra) to model the DMSO bulk. Vibrational frequencies computations were performed at the same level of theory to verify the stationary nature of the minima and the transition states, as well as to produce the zero-point energy (ZPE) and vibrational corrections to thermodynamic properties. Indeed, DFT is a ubiquitous tool in the bioinorganic chemistry [57–59] that allows accurate characterization of the structures and reaction pathways for the complexes with transition metals [60–62] including molybdenum [63]. The density functional ωB97XD is reputed to yield good geometrical structures and to precisely estimate the electronic energies [64,65].

The IEFPCM formalism was employed to account for solvation in water [66]. This method is known to yield free energies with

considerably smaller errors than continuum models, both for neutral and charged complexes, as recently demonstrated [67]. The IR spectra of $Mo_2(NSAID)_4$ complexes (vide infra) were calculated at the ωB97XD/def2SVP level of theory, either in gas or DMSO. The vibrational frequencies were shifted by the scaling factor 0.955 [68] and convoluted with a Lorentzian linewidth of 5.0 cm^{-1} by using the Molden software [69]. To enhance comparison, the calculated and experimental IR spectra were reported in percentage of absorbance with respect to the maximum absorbance band. Natural bond orbital analyses were performed by using the nbo7 code (NBO 7.0.9, 21-May-2020) integrated in the g16 execution flow [70]. The rendition of the isodensity surfaces for relevant frontier orbitals was carried out by using the Avogadro graphical interface (http://avogadro.cc; version 1.2.0) [71].

3.5. Cell culture

Human breast adenocarcinoma cells (MDA-MB-231) were purchased by European Collection of Authenticated Cell Cultures (ECACC; 92,020,424). Human lung carcinoma epithelial cells (A549, American Type Culture Collection, CCL-195), were kindly provided by Dr. R. Danesi, University of Pisa, Pisa, Italy. Human glioblastoma cells (U87MG) were purchased by CLS Cell Lines Service GmbH (Eppelheim, Germany).

MDA-MB-231 and A549 cells were maintained in DMEM-F12 (Corning) supplemented with 10% FBS (Corning), and U87MG in RPMI 1640 (Corning) supplemented with 10% FBS. All the media were supplemented with 2 mM L-glutamine, 100 U/mL penicillin, and 100 μg/mL streptomycin. Cells were maintained at 37 °C in a humidified 5% CO_2 atmosphere.

3.6. Cytotoxicity MTS assay

Cells were seeded in 96-well microplates (3.500 cells/well). After 24 h, cells were treated with different concentrations of the compounds. Compounds were dissolved in DMSO immediately before the beginning of the assay. The final DMSO concentration was 1%. The CTRL was treated with only DMSO at the same concentration. After 72 h of incubation, cell viability was determined using MTS assay (CellTiter 96 AQueous One Solution Cell Proliferation Assay kit; Promega) according to the manufacturer's instructions. The absorbance values at 490 nm were measured with the Ensight plate reader (Perkin Elmer).

3.7. Gene expression analysis

U87MG cells were seeded in 6-well microplates (350.000 cells/well). After 24 h, cells were treated with LPS (1 μg/mL) for 2 h and then complex 3 or aspirin were added and incubated for 48 h. At the end, cells were washed with Phosphate-buffered saline (PBS, Sigma Aldrich) and lysed. The total RNA was extracted using the RNeasy Mini Kit (Qiagen) according to the manufacturer's instructions. cDNA synthesis was performed with 1 μg of RNA using the i-Script cDNA synthesis kit (Bio-Rad) by following the manufacturer's instructions. The 20 μL real-time RT-PCR reactions mix consisted of 10 μL of SsoAdvanced Universal SYBR Green Supermix (Bio-Rad), 0.5 μL of 10 μM forward and reverse primers, 5 μL of cDNA (50 ng), and water. 40 cycles were performed using the protocol: 98 °C for 30 s and 60 °C for 30 s. The used primers were reported in Table 6 [72]. The relative mRNA levels were normalized against GAPDH used as housekeeping genes, and the relative expression was calculated by using the methods of the ΔΔCt by using the CFX Maestro Software (Bio-Rad).

3.8. Statistical analysis

The Graph-Pad Prism program (GraphPad Software Inc., San Diego, CA) was used for data analysis and graphic presentation. Statistical analysis was performed by ordinary one-way analysis of variance (ANOVA) with Bonferroni's multiple comparisons test. $P \leq 0.05$ was considered statistically significant.

Table 6
List of the used primers.

Gene	Sequence	Bp
GAPDH	FW 5′-GAGAAGTATGACAACAGCCT-3′ RV 5′-CCTTCCACGATACCAAAGTT-3′	107
IL-6	FW 5′-TCCTCGACGGCATCTTCA-3′ RV 5′-TTTTCACCAGGCAAGTCTCCT-3′	165
COX-2	FW 5′-TGTGTTGACATCCAGATCACAT-3′ RV 5′-GGAGTCGGGCAATCATCAGG-3′	141
NF-kB	FW 5′-CAGCAGATGGCCCATACCTT-3′ RV 5′-CACCATGTCCTTGGGTCCAG-3′	287

CRediT authorship contribution statement

Lorenzo Chiaverini: Investigation. **Valentina Notarstefano:** Writing – original draft, Supervision, Investigation. **Iogann Tolbatov:** Writing – original draft, Supervision, Investigation, Data curation. **Paolo Umari:** Writing – review & editing. **Elisabetta Giorgini:** Writing – review & editing. **Lidia Ciccone:** Writing – review & editing. **Riccardo Di Leo:** Writing – review & editing, Investigation. **Letizia Trincavelli:** Writing – review & editing. **Chiara Giacomelli:** Writing – review & editing, Writing – original draft, Investigation. **Laura Marchetti:** Investigation. **Tiziano Marzo:** Writing – review & editing, Writing – original draft, Supervision, Investigation, Funding acquisition, Data curation, Conceptualization. **Diego La Mendola:** Writing – review & editing, Writing – original draft. **Alessandro Marrone:** Writing – review & editing, Writing – original draft, Investigation, Formal analysis.

Declaration of competing interest

Tiziano Marzo reports financial support was provided by University of Pisa. Tiziano Marzo reports financial support was provided by Government of Italy. Diego La Mendola reports financial support was provided by University of Pisa. Iogann Tolbatov reports equipment, drugs, or supplies was provided by University of Burgundy. Iogann Tolbatov reports financial support was provided by European Union. Alessandro Marrone reports equipment, drugs, or supplies was provided by Interuniversity Consortium Cineca. Iogann Tolbatov reports financial support was provided by Council of the European Union. Tiziano Marzo reports equipment, drugs, or supplies was provided by University of Pisa. If there are other authors, they declare that they have no known competing financial interests or personal relationships that could have appeared to influence the work reported in this paper.

Data availability

Data will be made available on request.

Acknowledgements

TM, DLM thank the University of Pisa for the financial support under the Rating Ateneo funding program. TM thanks the financial support from Ministero Italiano dell'Università e della Ricerca (MUR) under the program PRIN 2022—Progetti di Rilevante Interesse Nazionale, project code: 2022ALJRPL "Biocompatible nanostructures for the chemotherapy treatment of prostate cancer". IT gratefully acknowledges the usage of HPC resources from Direction du Numérique – Centre de Calcul de l'Université de Bourgogne (DNUM CCUB). This work has been funded by the European Union - Next-Generation EU ("PNRR M4C2-Investimento 1.4- CN00000041"). We acknowledge the CINECA award under the ISCRA initiative, for the availability of high performance computing resources and support. V.N. acknowledges the received funding from the project Vitality – Project Code ECS00000041, CUP

I33C22001330007 - funded under the National Recovery and Resilience Plan (NRRP), Mission 4 Component 2 Investment 1.5 - 'Creation and strengthening of innovation ecosystems,' construction of 'territorial leaders in R&D' – Innovation Ecosystems - Project 'Innovation, digitalization and sustainability for the diffused economy in Central Italy – VITALITY' Call for tender No. 3277 of 30/12/2021, and Concession Decree No. 0001057.23-06-2022 of Italian Ministry of University funded by the European Union – NextGenerationEU. The authors wish to thank Dr. Beatrice Muscatello (Department of Pharmacy, University of Pisa), and the Center for Instrument Sharing of the University of Pisa (CISUP), University of Pisa, for the support with ESI-MS experiments.

Appendix A. Supplementary data

Supplementary data to this article can be found online at https://doi.org/10.1016/j.jinorgbio.2024.112697.

References

[1] F. Lupi, T. Marzo, G. D'Adamio, S. Cretella, F. Cardona, L. Messori, A. Goti, ChemCatChem 9 (22) (2017) 4225–4230.
[2] K. Skorda, G.S. Papaefstathiou, A. Vafiadis, A. Lithoxoidou, C.P. Raptopoulou, A. Terzis, V. Psycharis, E. Bakalbassis, V. Tangoulis, S.P. Perlepes, Inorg. Chim. Acta 326 (1) (2001) 53–64.
[3] I. Tolbatov, E. Barresi, S. Taliani, D. La Mendola, T. Marzo, A. Marrone, Inorg. Chem. Front. 10 (8) (2023) 2226–2238.
[4] M.A. Aquino, Coord. Chem. Rev. 170 (1) (1998) 141–202.
[5] L. Messori, T. Marzo, R.N.F. Sanches, D. de Oliveira Silva, A. Merlino, Angew. Chem. Int. Ed. 53 (2014) 6172–6175.
[6] E. Barresi, I. Tolbatov, T. Marzo, E. Zappelli, A. Marrone, N. Re, A. Pratesi, C. Martini, S. Taliani, F. Da Settimo, D. La Mendola, Dalton Trans. 50 (27) (2021) 9643–9647.
[7] R. Hrdina, Eur. J. Inorg. Chem. 2021 (6) (2021) 501–528.
[8] E. Barresi, I. Tolbatov, A. Pratesi, V. Notarstefano, E. Baglini, S. Daniele, S. Taliani, N. Re, E. Giorgini, C. Martini, F. Da Settimo, Dalton Trans. 49 (41) (2020) 14520–14527.
[9] C. Tolia, A.N. Papadopoulos, C.P. Raptopoulou, V. Psycharis, C. Garino, L. Salassa, G. Psomas, J. Inorg. Biochem. 123 (2013) 53–65.
[10] S. Fountoulaki, F. Perdih, I. Turel, D.P. Kessissoglou, G. Psomas, J. Inorg. Biochem. 105 (12) (2011) 1645–1655.
[11] A.L. Abuhijleh, J. Khalaf, Eur. J. Med. Chem. 45 (9) (2010) 3811–3817.
[12] A. Tarushi, S. Perontsis, A.G. Hatzidimitriou, A.N. Papadopoulos, D. P. Kessissoglou, G. Psomas, J. Inorg. Biochem. 149 (2015) 68–79.
[13] P. Edelsbacher, G. Redhammer, U. Monkowius, Monatsh. Chem. 151 (2020) 543–547.
[14] E.Y. Bivián-Castro, M. Flores-Alamo, R. Escudero, V. Gómez-Vidal, J.J. Segoviano-Garfias, J. Castañeda-Contreras, Q.E. Saavedra-Arroyo, Materials 16 (13) (2023) 4866.
[15] F. Vakil, I. Mantasha, M. Shahid, M. Ahmad, J. Struct. Chem. 60 (2019) 1971–1982.
[16] M. Iqbal, S. Ali, N. Muhammad, M. Sohail, Polyhedron 57 (2013) 83–93.
[17] V. Paredes-García, R.C. Santana, R. Madrid, A. Vega, E. Spodine, D. Venegas-Yazigi, Inorg. Chem. 52 (15) (2013) 8369–8377.
[18] A. Mushtaq, M. Iqbal, S. Ali, M.N. Tahir, Supramol. Chem. 33 (10) (2021) 616–623.
[19] A.N. Wein, R. Cordeiro, N. Owens, H. Olivier, K.I. Hardcastle, J.F. Eichler, J. Fluor. Chem. 130 (2) (2009) 197–203.
[20] G. Ribeiro, M. Benadiba, A. Colquhoun, D. de Oliveira Silva, Polyhedron 27 (3) (2008) 1131–1137.
[21] T. Yang, C.H. Wang, J. Zhang, S. He, A.P. Mouritz, Compos. Sci. Technol. 72 (12) (2012) 1396–1401.
[22] N.D. Knöfel, C. Schoo, T.P. Seifert, P.W. Roesky, Dalton Trans. 49 (5) (2020) 1513–1521.
[23] J. Wu, L. Miao, M. Yang, A. Li, Y. Cao, Q. Wang, J. Zhang, Z. You, Inorg. Chim. Acta 555 (2023) 121573.
[24] T. Tran, K. Krishnamoorthy, Y.W. Song, S.K. Cho, S.J. Kim, ACS Appl. Mater. Interfaces 6 (2014) 2980–2986.
[25] H. Pfeiffer, M. Dragoun, A. Prokop, U. Schatzschneider, Z. Anorg, Allg. Chem. 639 (8–9) (2013) 1568–1576.
[26] S.M. Pandey, J. Pandey, K. Saraswat, R. Kant, J. Indian Chem. Soc. 99 (11) (2022) 100759.
[27] H.Y. Khan, S. Parveen, I. Yousuf, S. Tabassum, F. Arjmand, Coord. Chem. Rev. 453 (2022) 214316.
[28] G. Malis, E. Geromichalou, G.D. Geromichalos, A.G. Hatzidimitriou, G. Psomas, J. Inorg. Biochem. 224 (2021) 111563.
[29] F. Jozefíková, S. Perontsis, K. Koňáriková, L. Švorc, M. Mazúr, G. Psomas, J. Moncol, J. Inorg. Biochem. 228 (2022) 111696.
[30] T.A. Stephenson, E. Bannister, G. Wilkinson, J. Chem. Soc. 1964 (1964) 2538–2541.
[31] E. Hochberg, P. Walks, E.H. Abbott, Inorg. Chem. 13 (8) (1974) 1824–1827.
[32] F.A. Cotton, J.G. Norman Jr., B.R. Stults, T.R. Webb, J. Coord. Chem. 5 (4) (1976) 217–223.
[33] S.M. Kuang, P.E. Fanwick, R.A. Walton, Inorg. Chem. Commun. 5 (2) (2002) 134–138.
[34] J.V. Brencic, F.A. Cotton, Inorg. Chem. 9 (2) (1970) 351–353.
[35] J. San Filippo, Inorg. Chem. 11 (12) (1972) 3140–3143.
[36] J. San Filippo, H.J. Sniadoch, R.L. Grayson, Inorg. Chem. 13 (9) (1974) 2121–2130.
[37] F.A. Cotton, T.S. Barnard, L.M. Daniels, C.A. Murillo, Inorg. Chem. Commun. 5 (7) (2002) 527–532.
[38] F.A. Cotton, D.D.O. Silva, Inorg. Chim. Acta 249 (1) (1996) 57–61.
[39] G. Socrates, Infrared and Raman Characteristic Group Frequencies: Tables and Charts, 3rd edition, John Wiley and Sons, Ltd, Chichester, UK, 2004.
[40] P. Larkin, Infrared and Raman Spectroscopy: Principles and Spectral Interpretation, Elsevier, Oxford, UK, 2011.
[41] R.J. Clark, A.J. Hempleman, M. Kurmoo, J Chem Soc, Dalton Trans. 1988 (4) (1988) 973–981.
[42] P.K. Kulkarni, M. Dixit, A. Jain, Stamford J Pharm Sci 4 (1) (2011) 1–8.
[43] H.M. Badawi, W. Förner, Spectrochim. Acta A Mol. Biomol. Spectrosc. 123 (2014) 447–454.
[44] R.J. Mureinik, J. Inorg. Nucl. Chem. 38 (7) (1976) 1275–1278.
[45] I.A. Squire, C.A. Goult, B.C. Thompson, E. Alexopoulos, A.C. Whitwood, T. F. Tanner, L.A. Wilkinson, Inorg. Chem. 61 (48) (2022) 19144–19155.
[46] W. Kosaka, N. Yamamoto, H. Miyasaka, Inorg. Chem. 52 (17) (2013) 9908–9914.
[47] I. Tolbatov, A. Marrone, Inorg. Chem. 61 (41) (2022) 16421–16429.
[48] L.A. Wilkinson, L. McNeill, P.A. Scattergood, N.J. Patmore, Inorg. Chem. 52 (16) (2013) 9683–9691.
[49] H. Endo, M. Yano, Y. Okumura, H. Kido, Cell Death Dis. 5 (1) (2014) e1027.
[50] V. Leidgens, C. Seliger, B. Jachnik, T. Welz, P. Leukel, A. Vollmann-Zwerenz, U. Bogdahn, M. Kreutz, O.M. Grauer, P. Hau, PLoS One 10 (10) (2015) e0140613.
[51] E. Bignon, M. Marazzi, V. Besancenot, H. Gattuso, G. Drouot, C. Morell, L. A. Eriksson, S. Grandemange, E. Dumont, A. Monari, Sci. Rep. 7 (1) (2017) 8885.
[52] M.M. Gilligan, A. Gartung, M.L. Sulciner, P.C. Norris, V.P. Sukhatme, D. R. Bielenberg, S. Huang, M.W. Kieran, C.N. Serhan, D. Panigrahy, Proc. Natl. Acad. Sci. 116 (13) (2019) 6292–6297.
[53] M.J. Frisch, G.W. Trucks, H.B. Schlegel, et al., Gaussian 16, Revision C.01, Gaussian, Inc., Wallingford CT, 2016.
[54] J.D. Chai, M. Head-Gordon, J. Chem. Phys. 128 (8) (2008) 084106.
[55] K.A. Peterson, D. Figgen, E. Goll, H. Stoll, M. Dolg, J. Chem. Phys. 119 (21) (2003) 11113–11123.
[56] F. Weigend, R. Ahlrichs, Phys. Chem. Chem. Phys. 7 (18) (2005) 3297–3305.
[57] R. Paciotti, I. Tolbatov, V. Graziani, A. Marrone, N. Re, C. Coletti, AIP Conf Proc 2040 (1) (2018), https://doi.org/10.1063/1.5079061. AIP Publishing.
[58] I. Tolbatov, N. Re, C. Coletti, A. Marrone, Inorg. Chem. 58 (16) (2019) 11091–11099.
[59] I. Tolbatov, A. Marrone, Theor. Chem. Accounts 140 (2) (2021) 20.
[60] R. Paciotti, I. Tolbatov, A. Marrone, L. Storchi, N. Re, C. Coletti, AIP Conf. Proc vol. 2186 (2019), https://doi.org/10.1063/1.5137922. No. 1. AIP Publishing.
[61] S. Todisco, M. Latronico, V. Gallo, N. Re, A. Marrone, I. Tolbatov, P. Mastrorilli, Dalton Trans. 49 (20) (2020) 6776–6789.
[62] I. Tolbatov, A. Marrone, Inorg. Chem. 61 (1) (2021) 746–754.
[63] M. Mohanty, G. Sahu, A. Banerjee, S. Lima, S.A. Patra, A. Crochet, G. Sciortino, D. Sanna, V. Ugone, E. Garribba, R. Dinda, Inorg. Chem. 61 (10) (2022) 4513–4532.
[64] I. Tolbatov, A. Marrone, R. Paciotti, N. Re, C. Coletti, Computational Science and Its Applications–ICCSA 2021, 2021, pp. 398–412. Part X 21 2021. Springer International Publishing, https://doi.org/10.1007/978-3-030-87016-4_30.
[65] I. Tolbatov, C. Coletti, A. Marrone, N. Re, Theor. Chem. Accounts 139 (12) (2020) 184.
[66] J. Tomasi, B. Mennucci, E. Cancès, J. Mol. Struct. THEOCHEM 464 (1–3) (1999) 211–226.
[67] A. Klamt, C. Moya, J. Palomar, J. Chem. Theory Comput. 11 (9) (2015) 4220–4225.
[68] J.C. Zapata Trujillo, L.K. McKemmish, Wiley Interdiscip Rev Comput Mol 12 (3) (2022) e1584.
[69] G. Schaftenaar, J.H. Noordik, J. Comput. Aided Mol. Des. 14 (2000) 123–134.
[70] NBO 7.0, E.D. Glendening, J.K. Badenhoop, A.E. Reed, J.E. Carpenter, J. A. Bohmann, C.M. Morales, P. Karafiloglou, C.R. Landis, F. Weinhold, Theoretical Chemistry Institute, University of Wisconsin, Madison, 2018.
[71] M.D. Hanwell, D.E. Curtis, D. Lonie, T. Vandermeersch, E. Zurek, G.R. Hutchison, J. Chemother. 4 (2012) 17.
[72] C. Giacomelli, L. Natali, M. Nisi, M. De Leo, S. Daniele, B. Costa, F. Graziani, M. Gabriele, A. Braca, M.L. Trincavelli, C. Martini, Stem Cell Res Ther 9 (1) (2018) 1–21.